HHS Public Access

Author manuscript

Brain Stimul. Author manuscript; available in PMC 2020 January 01.

Published in final edited form as:

Brain Stimul. 2019 ; 12(1): 129–138. doi:10.1016/j.brs.2018.10.004.

Limits and reproducibility of resting-state functional MRI definition of DLPFC targets for neuromodulation

Lipeng Ning[a,*], **Nikos Makris**[b], **Joan A Camprodon**[b,**], and **Yogesh Rathi**[a,**]

[a]Brigham and Women's Hospital, Harvard Medical School, USA.

[b]Massachusetts General Hospital, Harvard Medical School, USA.

Abstract

Background: Transcranial magnetic stimulation (TMS) is a noninvasive neuromodulation technique with therapeutic applications for the treatment of major depressive disorder (MDD). The standard protocol uses high frequency stimulation over the left dorsolateral prefrontal cortex (DLPFC) identified in a heuristic manner leading to moderate clinical efficacy. A proposed strategy to increase the anatomical precision in targeting, based on resting-state functional MRI (rsfMRI), identifies the subregion within the DLPFC having the strongest anticorrelated functional connectivity with the subgenual cortex (SGC) for each individual subject.

Objective: In this work, we comprehensively test the reliability and reproducibility of this targeting method for different scan lengths on 100 subjects from the Human Connectome Project (HCP) where each subject had a four 15-minute rsfMRI scan on 2 different days.

Methods: We quantified the inter-scan and inter-day distance between the rsfMRI-guided DLPFC targets for each subject controlling for a number of expected sources of noise using volumetric as well as surface analyses.

Results: Our results show that the average inter-day distance (with fMRI scans lasting 30 minutes on each day) is 25% less variable than the inter-scan distance, which uses 50% less data. Specifically, the inter-scan distance was more than 37 mm, while for the longer-scan, the inter-day distance had lower variability at 25 mm. Finally, we tested the same rsfMRI strategy using the nucleus accumbens (NAc) as a control region relevant to MDD but less susceptible to artifacts, using both volume and surface rsfMRI data. The results showed similar variability to the SGC-DLPFC functional connectivity. Moreover, our results suggest that a smoothing kernel with 12 mm full-width half maximum (FWHM) lead to more stable and reliable target estimates.

Conclusion: Our work provides a quantitative assessment of the topographic precision of this targeting method, describing an anatomical variability that may surpass the spatial resolution of

[*]Corresponding author: Lipeng Ning, Telephone: 617-525-6024, Fax: 617-525-6214, lning@bwh.harvard.edu. [**]Joint senior authors.

Conflicts of interest

This work has not been published and has not been submitted for publication elsewhere while under consideration. The authors declare no potential conflict of interest.

some forms of focal TMS as it is commonly applied, and provides recommendations for improved accuracy.

Keywords

Transcranial Magnetic Stimulation; Neuromodulation; functional connectivity; image-guided therapy; individualized therapy; precision medicine

1. Introduction

Transcranial magnetic stimulation (TMS) is a noninvasive brain stimulation technique with basic and clinical applications, including diagnostic and therapeutic uses [1]. In particular, high-frequency excitatory repetitive TMS (rTMS) to the left dorsolateral prefrontal cortex (DLPFC) has been validated as a safe and effective intervention for the treatment of major depressive disorder (MDD): it is approved by the U.S. Food and Drug Administration (FDA) since 2008 and it is part of the standard of care following national and international clinical guidelines [2, 3]. The most common strategy to identify the target of stimulation in the DLPFC is to center the TMS coil 5 cm anterior to the primary motor cortex representation of the hand, measured along the curvature of the scalp (the “5cm rule”). While this approach, developed on the basis of population-based morphometric analyses, was sufficient to separate active TMS from placebo in large clinical trials, it is certainly inaccurate for a number of reasons. Using an absolute distance (i.e. 5cm) introduces an obvious bias related to head size, as larger heads should require a greater distance between the motor cortex and DLPFC. Indeed, Herwig and colleagues [4] demonstrated that the 5cm rule leads to targets that are inaccurately dorsal and/or posterior in 68% of all subjects. Importantly, other studies have demonstrated that this anatomical imprecision is clinically relevant: [5] analyzed the location of stimulation for the OPT-TMS trial [3], a large multicenter randomized placebo-controlled trial of TMS for the treatment of MDD, and determined that all subjects who had been stimulated too posteriorly (in pre-motor regions) following the 5cm rule failed to respond to treatment. Similar analyses of trials using the “5cm rule” have identified that more anterior targets are associated with better clinical response [6]. These data provide evidence that anatomical differences are indeed determinant for the therapeutic efficacy of TMS, and that the 5cm rule is a source of error that can lead to inappropriate coil positioning with negative implications for efficacy.

Small trials using image-guided TMS with stereotactic neuronavigation have shown that increasing the anatomical specificity and intersession reliability of stimulation could potentially improve clinical efficacy [7, 8]. Although image-guided neuronavigation is standard in cognitive or systems neuroscience, leading to greater anatomical precision and behavioral effect size [9], it is still rare in clinical practice. This is partly due to the size and heterogeneity of the DLPFC, a large structure with very diverse functions and patterns of connectivity [10]. Most attempts to prospectively investigate the use of neuronavigation in therapeutic antidepressant trials have used the boundary between Broadman areas 46 and 9 (BA46/9) as the target of stimulation. This approach, while potentially more reliable due to the use of neuronavigation, is still based on populationbased maps (as we do not measure cytoarchitectonic properties for each subject but use population-based atlases) and continues

to lack the specificity of the true individual anatomy of each subject. Further, the evidence pointing to BA46/9 as the ideal target for TMS modulation of circuits pathologically involved in MDD is not strong, primarily because while there may be a relationship between cytoarchitectonics and function, the overlap between the structural and functional anatomy of multimodal association cortices such as the DLPFC is variable and imprecise across individuals [11, 12]. Cytoarchitectonically defined landmarks are thus unlikely to provide the functional specificity and individualized resolution needed. Therefore, the need for precision-medicine strategies for TMS target identification is still an unresolved problem, though one that is expected to significantly increase the therapeutic efficacy of this intervention.

Functional-connectivity has been proposed as an individualized strategy to identify DLPFC targets on the basis of known circuit-based anatomy and patterns of functional coherence. The subgenual cingulate cortex (SGC) is a critical node in the patho-physiology of MDD, with multiple layers of mechanistic and clinical evidence suggesting its involvement in the maladaptive development of the affective, autonomic and behavioral symptoms of MDD. Specifically, the SGC has been shown to be hyperactive in the context of MDD, and this pathological signal normalizes after effective treatment [13, 14, 15]. The DLPFC has also been critically involved in the pathophysiology of MDD, particularly related to executive symptoms and faulty homeostatic control of affective states [16]. Unlike SGC, the DLPFC has been shown to be hypoactive in active depression, and this pattern also tends to normalize after effective treatment [17, 14, 16, 18].

The anticorrelated relationship between DLPFC and SGC has been captured using resting-state functional connectivity analyses of low-frequency BOLD signal oscillation. Retrospective analyses have suggested that the antidepressant efficacy of rTMS is correlated to the functional connectivity between the left DLPFC and the SGC, thus suggesting the use of the node in the left DLPFC that was most anti-correlated with SGC as a subject-specific stimulation target [19]. An initial assessment of the reliability of the rsfMRI-guided approach on a small number of subjects showed that the intra-subject SGC-DLPFC functional connectivity map was better correlated with the functional connectivity (FC) map obtained from the same subject on a different day than that of a group-average FC map [20]. Although the general reliability of brain networks determined by FC maps and related measures have been investigated in several prior studies [21, 22, 23, 24], the intrinsic variability of the specific SGC-DLPFC maps and the corresponding brain targets has not been determined to date using large data sets. Quantifying the spatial variability of the subject-specific rsfMRI-guided target is important for understanding the reliability and reproducibility of target definition strategies. A reliable localization methodology is expected to produce nearly the same brain stimulation target from data acquired in different sessions. Excessive intra-subject variability in the identification of the target, particularly if it is beyond the spatial resolution of the stimulation technique, could lead to highly variable therapeutic results. Thus, high reproducibility is critical for the clinical efficacy of rTMS in depression.

In this paper, we study the *intra-subject* variability of rsfMRI-guided target using data set from the Human Connectome Project (HCP) [25]. We analyzed the SGC-DLPFC functional

connectivity maps from 100 HCP subjects where each subject had four 15-minute rsfMRI scans on 2 different days. Our results showed that the inter-scan Euclidean distance between the rsfMRI-guided target region was more than 38 mm. The brain targets identified using a combination of two scans from the same day, which is equivalent to a 30-minute scan session, has lower variability, but still with an inter-day distance larger than 25 mm. Considering that the rsfMRI signal in the SGC region usually has a slightly lower signal to noise ratio [26], we also tested the reproducibility of FC map using a control seed region in the nucleus accumbens (NAc) using both volume and surface data with different preprocessing methods. The inter-scan and inter-day results were consistent with those obtained for the SGC-DLPFC connectivity.

2. Methods

2.1. Subjects and data

We analyzed the data set from 100 unrelated subjects from HCP [25], where the subjects include 46 male and 54 female with ages ranging from 22 to 36 years. Each subject had four 15-minute scan data provided in both volume and surface data formats in the MNI space from two contiguous days with two runs from each day. A warp transform is also provided for converting the volume data from MNI space to the native T1w space. The acquisition parameters for rsfMRI data were TE = 33 ms, TR = 0.72 s, with a multi-band factor of 8. The volume data had 2 mm isotropic voxel size. Moreover, the T1w image had a higher spatial resolution with 0.7 mm isotropic voxels. More information about data acquisition and preprocessing can be found in [27].

2.2. Functional connectivity data pre-processing and analysis

For one of our analysis, we used the volumetric minimally processed rsfMRI data, which is corrected for various distortions and head motion [28]. Following the methodology given in [29], the data was then processed using SPM12 (Well-come Department of Cognitive Neurology, London, UK) using the following parameters: i) drop 4 initial volumes, ii) smooth the data using a Gaussian kernel with 4 mm FWHM, iii) filter the data using a filter with pass band between 0.01 and 0.08 Hz, iv) regress-out nuisance signals from the white-matter and CSF regions using label maps provided by HCP, and v) regress-out the global average signal from all voxels. We note that the HCP pipeline corrects for head motion. Slice-timing correction is not necessary for these data sets due to the low TR [30]. For the surface data, we used the data that had been processed by the HCP ICA-FIX pipeline where non-neural spatiotemporal components in the signal were removed from the minimally processed data [30]. Similar to the volume data, we also applied the global signal regression (GSR) from the surface data before computing the FC maps, since GSR could improve the spatial specificity of functional connectivity maps [31, 32].

The SGC seed region was defined by manually drawing a line in the sagittal plane bordering with the most rostral point of the genu of the corpus callosum, and including the entire subgenual cortex (in the cingulate and ventral to it) posterior to this border and excluding the white matter area. Since this seed region does not project properly to the surface space, we only analyzed the SGC FC maps using the volume data. Fig. 1 illustrates the SGC ROI of an

HCP subject on a slice that is 3.65 mm left lateral from the sagittal plane. This SGC ROI is slightly different from the one proposed in [19, 20] where it was defined by a 10-mm radius sphere centered at MNI coordinates (6,16,10). Of note, the rsfMRI signal in the SGC region usually has lower signal to noise ratio [26] due to susceptibility artifacts, although this is corrected by the distortion correction algorithm during the minimal processing of the HCP data [30]. In order to determine the influence of EPI distortions on our results, we selected another critical disease-relevant node (as a control region), the Nucleus Accumbens (NAc), located in the subcortical depth of the parenchyma and critically involved in processing anhedonia, amotivation and positive affect dimensions of MDD. Automated atlas-based parcellations using FreeSurfer [33] was used to define the NAc for every individual subject. The NAc FC maps were computed using both volume and surface data. Since the volume rsfMRI data is provided in the standard MNI space, the corresponding FC maps were also initially computed in the standard MNI space and were transformed to the native T1w space using the provided warp transforms.

The target for TMS was defined as a voxel in the left DLPFC with the strongest anticorrelated activity with the SGC. We combined the pars triangularis, rostral middle frontal, caudal middle frontal, superior frontal, lateral orbitofrontal, and the frontal pole regions provided by FreeSurfer [33] to define our larger DLPFC search area. Given the large surface of the DLPFC, the localization of the most negative voxels or vertices in the FC maps is clearly sensitive to measurement noise. In order to improve the robustness of rsfMRI-guided target, we spatially smoothed the FC maps, instead of rsfMRI data, using a Gaussian kernel with different values of FWHM, ranging from 4 mm to 24 mm. The lower bound 4 mm was selected because the spatial specificity of BOLD fluctuations measured at 3T is around 4 mm [34, 27]. An FWHM of 24 mm corresponds to the magnetic field intensity of a standard figure-8 TMS coil whose intensity decreases to around 75% of the maximum at a distance of 12 mm [35, 20]. The volumetric FC maps were smoothed using the SPM12 package and the Connectome Workbench was used for smoothing the surface FC maps.

To assess the benefits of using more data in determining the rsfMRI-guided target, we also concatenated the two 15-minute scans from the same day to compute a single FC map (equivalent to a single 30-minute session), and obtained two FC maps for each subject. The same smoothing approach was applied to process the FC maps from the two 30-min sessions. From the smoothed FC maps, the intra-subject variability was then characterized by several quantitative measures described in the next section.

2.3. Quantitative measures for intra-subject variability

2.3.1. Distance between rsfMRI-guided targets—For each of the SGC-DLPFC functional connectivity maps (four scan sessions), we first identified the coordinate (voxel) with the most negative correlation in the DLPFC region. Then, we computed the distance between the coordinates estimated from each pair from the 4 FC maps, resulting in a total of 6 distance measures. Though the distance between dominant peaks may be sensitive to measurement noise in the FC maps, the Gaussian smoothing kernel with different values of FWHM in pre-processing could potentially reduce estimation error and strengthen the

magnitude of the dominant peaks. The average of these 6 distances is defined as the *inter-scan distance* between the rsfMRI-guided targets. Similarly, we also computed the distance between the rsfMRI-guided targets from the 2 FC maps given by the two 30-min rsfMRI sessions. The corresponding distance is defined as the *inter-day distance*. These distance measures were computed in the native subject space of the T1w images. The FC maps were then transformed into the surface space for visualization.

For the NAc-DLPFC functional connectivity maps (our control region), there is no sufficient evidence to define an a priori preference for positive or negative functional connectivity peaks. Thus, we computed the coordinates for both, the positive and negative peaks, and estimated the distance between the respective peaks. The distance computed using the volumetric FC maps were computed in the native subject space, while the distance from surface FC maps was in the standard MNI space (note: distances were not computed on inflated surfaces).

2.3.2. Spatial correlation between FC maps—While the above distance measure between dominant peaks provides a quantitative metric to understand the reliability of rsfMRI-guided target in rTMS, these measures do not reveal the large-scale reproducibility of FC maps. To quantify the variability of entire FC maps (and not just the peaks), we computed the correlation coefficient (CC), r, between each pair of the 4 FC maps in the entire DLPFC region from each rsfMRI scan and between the 2 FC maps from two different days, respectively. The mean value of the correlation coefficient is referred as the *inter-scan consistency* and *inter-day consistency*, respectively. The consistency measures take values between −1 and 1. Highly reproducible FC maps should have a consistency measure close to one. Then, the Fisher z-transform was applied to transform the correlation coefficients r to $z(r)$. The mean and standard deviation of $z(r)$, i.e. $\bar{z}$, and z_{std}, were computed from the 100 subjects. Then, the Fisher inverse z-transform of $\bar{z}$ and $\bar{z} \pm z_{\text{std}}$ determine the mean and the variance of r.

We note that the above definition of inter-scan distance/consistency not only contain information on the difference between FC maps from intra-day rsfMRI scans but also the inter-day rsfMRI scans. To understand the difference between the intra-day and inter-day rsfMRI scans, we have also computed an alternative inter-scan distance/consistency by only comparing two pairs of FC maps from rsfMRI data acquired on the same day. But the results are very similar to the above definition of inter-scan distance by using all the 6 pairs of FC maps, see the Supplementary Material. Therefore, we only report the inter-scan distance/consistency from based on the 6 pairs of FC maps in below.

3. Results

3.1. SGC-DLPFC functional connectivity

The solid blue and red lines in Fig. 2a illustrate the mean value for the inter-scan and inter-day distance for the SGC-DLPFC functional connectivity maps, respectively. As noted earlier, we varied the size of the smoothing kernel (FWHM) to see its effect on the resulting connectivity maps. The dashed lines are the corresponding ± standard deviation plots. We note that the inter-scan distance does not change much for different FWHM values. Its

minimum value is 37.4 mm which is obtained at FWHM=12 mm. We also note that the inter-day distance using 30-min data is always smaller than the inter-scan distance using 15-min data where the p-value (t-test) reduces from 0.016 to 9×10^{-6} as the FWHM increases from 4mm to 24mm, which shows the benefit of using more measurements and larger smoothing kernels. The inter-day distance reduces from 34.2 mm to 26.3 mm as FWHM changes from 4 mm to 12 mm. There is no significant improvement when using larger smoothing kernels. We note that the smoothing kernel also reduces the strength of correlation coefficients.

Fig. 2b shows the mean (solid lines) and standard deviation (dashed lines) of the correlation coefficient of the most negative peaks of the SGC-DLPFC FC maps. The strength of the CC decreases with increasing FWHM, due to smoothing effects. The most negative values for inter-scan and inter-day CC were 0.39 and 0.33, respectively.

Fig. 2c shows the consistency of the FC maps. As expected, the inter-day consistency is always higher than inter-scan consistency ($p < 0.003$), and both consistency measures monotonically increase with higher values for FWHM. We also note that the values for the consistency measures are similar to those reported in [20]. As an example, Figs. 3a and 3b illustrate the FC maps from the 4 scans of the same subject smoothed by Gaussian kernels with FWHM=4 mm and 12 mm, respectively. Figs. 4a and 4b show the corresponding FC maps on two different days. Clearly, these FC maps show strong variability for the location of the dominant negative peaks.

3.2. NAc-DLPFC functional connectivity

To check if the rsfMRI signal in NAc has better quality than SGC, we computed the signal to noise ratio (SNR) using the approach described in [36]. The SNR in the SGC and NAc regions was 11.5 and 16.9, respectively. The lower SNR in SGC may be caused by stronger susceptibility artifacts in that region [26]. The inter-scan (15-min) and inter-day (30-min) distances for the NAcDLPFC maps for the positive and negative peaks from the volumetric data are shown in Figs. 5a and 5b, respectively. The inter-day distances between positive peaks are consistently smaller than the inter-scan distances ($p < 0.038$). The values of the most negative and most positive peaks are shown in Figs. 5c and 5d, respectively. The rsfMRI consistency measures for the NAc-DLPFC FC maps are shown in Fig. 5e where the inter-day consistency is higher than the inter-scan consistency ($p < 0.0005$). We note that the consistency measure in Fig. 5e reflects the variability of the entire DLPFC region, which is not separated into positive or negative values.

Similar to the SGC-DLPFC maps, the inter-scan distance is larger than the inter-day distance while the inter-day consistency is higher. We also note that the distance between positive peaks is much smaller than the distance between negative peaks, indicating that there may exist an intrinsic positive correlation between DLPFC and NAc. The minimum inter-scan and inter-day distances of negative peaks are 45.0 mm and 41.8 mm, which are obtained for FWHM=8, 4 mm, respectively. The minimum of both inter-scan and inter-day distances between positive peaks was obtained for FWHM=12 mm. The corresponding minimal values were 33.2 mm and 25.0 mm, respectively. The maximum values of inter-scan and inter-day CC from Fig. 5c are equal to 0.35 and 0.30, respectively. The corresponding values

in Fig. 5d are equal to 0.33 and 0.26, respectively. Thus, the positive CC also has higher strength than the negative values.

Figs. 6a and 6b show the distance between the peaks for the NAc-DLPFC maps using the surface data and the pial surfaces for each subject provided by the HCP dataset. Figs. 6c and 6d illustrate the most positive and negative values of FC maps, respectively. We note that the strength of the CC is much smaller than those illustrated in Figs. 5c and 5d. Fig. 6e shows the corresponding consistency measures for the entire DLPFC region. Very different from the results from volume data, the inter-day distance is no longer smaller than the inter-scan distance. Further, both distance measures are around 40 mm for different FWHM and larger than that obtained from volumetric data.

3.3. Compare SGC-DLPFC and NAc-DLPFC functional connectivity

To understand if the SGC-DLPFC and NAc-DLPFC FC maps have peak values in a similar region of DLPFC, we also computed the distance between the corresponding peaks using FC maps obtained from the volume data. Fig. 7a illustrates the distance between the negative peaks of SGC-DLPFC FC maps and the positive peaks of the NAc-DLPFC maps for different values of FWHM. The distance is more or less constant with varying FWHM. The minimum inter-scan and inter-day distances are 40.9 mm and 39.9 mm, respectively. Fig. 7b shows the distance between the most negative peaks of SGC-DLPFC and NAc-DLPFC maps. The distances have much higher values than the results shown in Fig. 7a. Moreover, the distances in Fig. 7b are increasing with FWHM. The minimum values of inter-scan and inter-day distances are 48.4 mm and 46.4 mm, respectively.

4. Discussion

In this work, we used high-quality and high-resolution HCP data from 100 subjects to assess the reliability rsfMRI-guided target localization for DLPFC neuromodulation in MDD. Different from most early works that consider the general reproducibility of FC-map based brain networks [21, 22, 23, 24, 37], this paper focuses on quantifying the intra-subject reproducibility and variability of the specific SGC-DLPFC and NAc-DLPFC FC maps which are important in TMS therapy in MDD. From the analysis of rsfMRI data from four scan sessions acquired on two consecutive days, the most topographically reliable targets were identified using two 15-minute scans and a 12 mm FWHM smoothing kernel, leading to 26.3 mm intra-subject variability. Using a single 15-minute scan instead lead to 37.4 mm (SGC) and 33.2 mm (NAc) variability. Of note, the variability of target is expected to be even larger if the sites are mapped from the cortical surface on to the scalp surface. Though the reliability of the SGCDLPC FC maps could possibly be impact by the choice of seed region, the NAc-DLPFC FC maps have similar results, despite differences in SNR, susceptibility artifacts and the choice of seed regions. The FC maps in volume space were more reliable than surface-based analyses for the NAc-DLPFC maps, which is reflected by the smaller distance measures and higher consistency provided by volume data. Moreover, positively correlated DLPFC targets with the NAc were more reliable than anticorrelated nodes.

4.1. Smoothing kernel: the role of preprocessing

All analyses show consistently that the 12 mm FWHM smoothing kernel of the FC maps leads to more stable and least variable DLPFC targets. While this is a wider smoothing kernel than commonly used in fMRI analyses, it may be the best pre-processing strategy when using rsfMRI for the specific application of identifying cortical neuromodulation targets. The more standard 4–6 mm smoothing kernels typically applied to smooth rsfMRI data had similar inter-scan (39.6 mm vs. 37.4 mm) but worse inter-day variability (34.2 mm vs. 26.3 mm). Moreover, the standard smoothing generally leads to low consistency measures, which further supports the lack of reproducibility of FC maps. But a larger FWHM could reduce the influence of suspicious local maxima of correlation maps and increase the reproducibility. This finding highlights the value of exploring different smoothing and pre-processing strategies in other image-guided fMRI applications (e.g. pre-surgical mapping for resections or device-based neuromodulation).

4.2. Inter-scan vs. inter-day measures: the role of data acquisition and quality

Volumetric analyses revealed that inter-session differences, with two 15-minute scans (a total of 30 minutes), were approximately 25% more reliable than inter-scan assessments using a single 15 minute run (i.e. 50% less data). This suggests that a strategy to improve target reliability could be to simply increase the data quality with more data points, which could be accomplished with longer scan duration, a greater number of sessions or more efficient pulse sequences able to acquire more data in less time. All these strategies have potential counterproductive weaknesses though (e.g. increased risk for motion) and should be empirically tested and validated for the purpose of rsfMRI DLPFC target identification. We note though that, using a higher magnetic field, e.g. 7T, could increase data quality without increasing acquisition time. In addition, it is also likely that there exists a resolution limit for the brain target, whose localization variability cannot be further reduced after the data quality reaches a ceiling points. Future studies should explore the limits of the spatial precision for localizing brain target for TMS by exploring data sets with different sizes. Finally, we note another important factor that limits the reliability of rsfMRI-guided target is the temporally varying cognitive states which leads to dynamic FC maps [38, 39, 40]. A suitable approach to remove the influence of different cognitive states could potentially improve the reliability of FC maps [41].

4.3. Variability across seeds: SGC vs. NAc

Since we did not have strong a priori assumption about the optimal pattern of functional connectivity from the NAc to the DLPFC, we explored both positively and negatively correlated maps. We observed that positive correlations were more topographically reliable with 25.0 mm intra-subject variability instead of 41.8 mm for negative correlations (both using inter-day differences, which were better than inter-scan). Interestingly, a more narrow smoothing kernel (4 mm) showed a slight advantage in topographical precision over 12 mm for negatively correlated nodes only, though still significantly worse than positive correlation maps. Positive correlation maps were most reliable at 12 mm smoothing, so we used these as a comparison to the SGC maps and targets.

We did not observe any difference in topographic accuracy between the targets defined from the SGC seed, an area with particularly problematic susceptibility artifacts and lower SNR [26], and the NAc seed, which is deeper in the parenchyma and less susceptible to these data acquisition problems. This is likely to be a reflection of the quality of the preprocessing, including the strategies leading to the HCP minimally processed dataset [30]. Interestingly, analyses in volume space were more reliable than in surface, and the differences between inter-day and inter-scan were negligible in surface space (both equally bad), which may be caused by the difference preprocessing methods (temporal filtering vs. ICA-FIX).

The NAc is an important node in the meso-cortico-limbic reward circuitry, which is pathologically affected in MDD [42]. It is thought to be involved in the maladaptive processes leading to anhedonia, amotivation and more global deficits in positive affect, common in many patients with depression [43, 44, 45]. The mean distance between the SGC and NAc targets in the DLPFC was 40.9 mm (inter-scan) and 39.9 mm (inter-day), likely beyond the resolution of TMS using common coils and parameters [46]. This suggests that the SGC and NAc maps could identify different DLPFC stimulation strategies likely to modulate distinct networks involved in depression. Given that the reliability of NAc targets is equal to that of SGC, this may be an alternative strategy for rsfMRI-guided therapeutic modulation. Future studies should test this approach in patients with MDD, but also in other neuropsychiatric populations with reward circuit dysfunction (e.g. substance use disorders or schizophrenia with prominent negative symptoms). Of note, the strength of (negative) connectivity between the DLPFC and SGC was greater than the (positive) correlations between the DLPFC and the NAc (0.39 v.s. 0.35). The clinical significance of this result needs to be considered.

4.4. Conclusions

Our results provide a quantitative assessment of the topographic precision and variability of rsfMRI functional connectivity to identify DLPFC targets for neuromodulation based on SGC and NAc seeds. The most reliable strategy using two 15 minute scans and a pre-processing with 12 mm FWHM smoothing leads to an intra-subject variability of 25 mm. Our data identified a number of methodological variables (data quality and pre-processing strategies) that impact the reliability of this targeting strategy. It also confirms that commonly used approaches to identify DLPFC targets based on functional connectivity (using runs of 5–10 minutes duration with longer TRs, hence with considerably fewer data points, smoothing rsfMRI data using of 4 – 8 mm kernels and no smoothing of the FC maps) could be significantly less reliable (with intra-subject variability in the order of 40 mm or greater) leading to inaccurate targeting and less effective neuromodulation.

The spatial resolution of TMS depends on a number of variables, such as coil architecture, coil orientation, pulse intensity and individual head and brain anatomy, among others [47, 48, 46, 49]. While the surface of the stimulated cortical area can indeed vary as a function of TMS parameters and individual variables, it should be smaller than the topographical variability we describe for common rsfMRI-based targeting strategies (e.g. 6 mm smoothing using short scans with long TRs - so few data points - and no smoothing of FC maps). This means that rsfMRI targeting strategies are likely to have a topographical variability larger

than the actual spatial resolution of TMS, implying that the desired target may not always be stimulated. That said, these individualized targeting strategies may still be more accurate than using population-based skull measures such as the “5cm rule”. Individualized modeling, or empirical assessments, of the TMS-induced electric field may be an important additional step to maximize the efficacy of target and network modulation with TMS. On the other hand, although our best performing strategy is not commonly used for TMS targeting, it provides a significantly improved topographic reliability which may be sufficient for certain TMS protocols. Further work is needed to prospectively explore data acquisition and analysis strategies to further improve the topographic reliability of TMS target definition with rsfMRI, and importantly, to integrate this with assessments of the focallity and topography of the electric field induced by TMS and other neuromododulation devices.

Future research should further explore the impact of data quality and pre-processing algorithms on target variability, and determine if the topographic precision could be improved even further. It should also be considered that functional MRI measures the BOLD signal, a proxy for brain activation and physiology. Physiology is variable by definition, particularly in high order association or limbic structures which fluctuate as a function of internal states and external demands, in both health and disease. Our analyses used data from 100 healthy young individuals, but older age and disease states may further impact the precision of this targeting strategy. Therefore, it is possible that at least part of the observed variability is not simply technical artifactual noise, but the actual true accurate measurement of a dynamic biological signal. Alternative approaches focused on more naturally stable biological properties, such as structural connectivity and tractographic anatomy, may represent a more reliable alternative for image-guided neuromodulation, if confirmed with prospective MRI-guided TMS studies.

Supplementary Material

Refer to Web version on PubMed Central for supplementary material.

Acknowledgement

The authors would like to acknowledge the following grants which supported this work: Brain and Behavior Research Foundation (NARSAD) to JAC and NIH grants R01MH112737, R21AG056958 to JAC, R21DA042271 to NM and JAC, R21MH113018 to LN and JAC and R01MH097979 to YR.

References

[1]. Camprodon J, Transcranial magnetic stimulation, in: Camprodon J, Rauch S, Greenberg B, Dougherty D (Eds.), Psychiatric Neurotherapeutics: Contemporary Surgical & Device-Based Treatments in Psychiatry, Humana Press (Springer), 2016.

[2]. O’Reardon J, Solvason H, Janicak P, Sampson S, Isenberg K, Nahas Z, McDonald W, Avery D, Fitzgerald P, Loo C, Demitrack M, George M, HA S, Efficacy and safety of transcranial magnetic stimulation in the acute treatment of major depression: a multisite randomized controlled trial, Biol. Psychiatry 62 (11) (2007) 1208–1216. [PubMed: 17573044]

[3]. George M, Lisanby S, Avery D, McDonald W, Durkalski V, Pavlicova M, Anderson B, Nahas Z, Bulow P, Zarkowski P, Holtzheimer PI, Schwartz T, Sackeim H, Daily left prefrontal transcranial magnetic stimulation therapy for major depressive disorder: a sham-controlled randomized trial, Arch Gen Psychiatry 67 (5) (2010) 507–516. [PubMed: 20439832]

[4]. Herwig U, Padberg F, Unger J, Spitzer M, Schönfeldt-Lecuona C, Transcranial magnetic stimulation in therapy studies: Examination of the reliability of “standard” coil positioning by neuronavigation, Biol. Psychiatry 50 (1) (2001) 58–61. [PubMed: 11457424]

[5]. Johnson M, an Baig KA, Ramsey D, Lisanby S, Avery D, McDonald X, ad Li WM, Bernhardt E, Haynor D, Holtzheimer PI, Sackeim H, George M, Nahas Z, Prefrontal rTMS for treating depression: location and intensity results from the OPT-TMS multi-site clinical trial, Brain Stimul. 6 (2) (2013) 108–117. [PubMed: 22465743]

[6]. Herbsman T, Avery D, Ramsey D, Holtzheimer P, Wadjik C, Hard-away F, Haynor D, George M, Nahas Z, More lateral and anterior prefrontal coil location is associated with better repetitive transcranial magnetic stimulation antidepressant response, Biol Psychiatry. 66 (5) (2009) 509–515. [PubMed: 19545855]

[7]. Fitzgerald P, Hoy K, McQueen S, Maller J, Herring S, Segrave R, Bailey M, Been G, Kulkarni J, Daskalakis Z, A randomized trial of rTMS targeted with MRI based neuro-navigation in treatment-resistant depression, Neuropsychopharmacology 34 (5) (2009) 1255–1262. [PubMed: 19145228]

[8]. Schönfeldt-Lecuona C, Lefaucheur J, Cardenas-Morales L, Wolf R, Kammer T, Herwig U, The value of neuronavigated rTMS for the treatment of depression, Neurophysiol Clin 40 (1) (2010) 37–43. [PubMed: 20230934]

[9]. Sack A, Kadosh R, Schuhmann T, Moerel M, Optimizing functional accuracy of TMS in cognitive studies: a comparison of methods, Journal of Cognitive Neuroscience 21 (2) (2009) 207–221. [PubMed: 18823235]

[10]. Petrides M, Pandya D, Dorsolateral prefrontal cortex: comparative cytoarchitectonic analysis in the human and the macaque brain and corticocortical connection patterns, European Journal of Neuroscience 11 (3) (1999) 1011–36. [PubMed: 10103094]

[11]. Rajkowska G, Goldman-Rakic P, Cytoarchitectonic definition of prefrontal areas in the normal human cortex: I. Remapping of areas 9 and 46 using quantitative criteria, Cerebral Cortex 5 (4) (1995) 307–322. [PubMed: 7580124]

[12]. Wang D, Buckner RL, Fox MD, Holt DJ, Holmes AJ, Stoecklein S, Langs G, Pan R, Qian T, Li K, Baker JT, Stufflebeam SM, Wang K, Wang X, Hong B, Liu H, Parcellating cortical functional networks in individuals, Nature Neuroscience 18 (2015) 1853–1860. [PubMed: 26551545]

[13]. Drevets W, Savitz J, Trimble M, The subgenual anterior cingulate cortex in mood disorders, CNS Spectr. 13 (8) (2008) 663–681. [PubMed: 18704022]

[14]. Mayberg H, Modulating dysfunctional limbic-cortical circuits in depression: towards development of brain-based algorithms for diagnosis and optimised treatment, British Medical Bulletin 65 (1) (2003) 193–207. [PubMed: 12697626]

[15]. Mayberg H, Lozano A, Voon V, McNeely H, Seminowicz D, Hamani C, Schwalb J, Kennedy S, Deep brain stimulation for treatment-resistant depression, Neuron 45 (2005) 651–660. [PubMed: 15748841]

[16]. Koenigs M, Grafman J, The functional neuroanatomy of depression: distinct roles for ventromedial and dorsolateral prefrontal cortex, Behav Brain Res 201 (2) (2009) 239–243. [PubMed: 19428640]

[17]. Mayberg H, Limbic-cortical dysregulation: A proposed model of depression, J Neuropsych Clin Neurosci 9 (1997) 471–481.

[18]. Price J, Drevets W, Neurocircuitry of mood disorders, Neuropsychopharmacology 35 (1) (2010) 192–216. [PubMed: 19693001]

[19]. Fox M, Buckner R, White M, Greicius M, Pascual-Leone A, Efficacy of transcranial magnetic stimulation targets for depression is related to intrinsic functional connectivity with the subgenual cingulate, Biol. Psychiatry 72 (2012) 595–603. [PubMed: 22658708]

[20]. Fox M, Liu H, Pascual-Leone A, Identification of reproducible individualized targets for treatment of depression with tms based on intrinsic connectivity, NeuroImage 66 (2013) 151–160. [PubMed: 23142067]

[21]. Wisner KM, Atluri G, Lim KO, MacDonald AW, Neurometrics of intrinsic connectivity networks at rest using fMRI: Retest reliability and cross-validation using a meta-level method, NeuroImage 76 (Supplement C) (2013)236–251. [PubMed: 23507379]

[22]. Birn RM, Molloy EK, Patriat R, Parker T, Meier TB, Kirk GR, Nair VA, Meyerand ME, Prabhakaran V, The effect of scan length on the reliability of resting-state fmri connectivity estimates, NeuroImage 83 (Supplement C) (2013) 550–558. [PubMed: 23747458]

[23]. Termenon M, Jaillard A, Delon-Martin C, Achard S, Reliability of graph analysis of resting state fmri using test-retest dataset from the human connectome project, NeuroImage 142 (Supplement C) (2016) 172–187. [PubMed: 27282475]

[24]. Bouix S, Swago S, West JD, Pasternak O, Breier A, Shenton ME, “evaluating acquisition time of rfmri in the human connectome project for early psychosis. how much is enough?”, in: Wu G, Laurienti P, Bonilha L, Munsell BC (Eds.), Connectomics in NeuroImaging, Springer International Publishing, Cham, 2017, pp. 108–115.

[25]. Van Essen DC, Smith SM, Barch DM, Behrens TE, Yacoub E, Ugurbil K, The WU-Minn human connectome project: an overview, Neuroimage 80 (2013) 62–79. [PubMed: 23684880]

[26]. Ojemann J, Akbudak E, Snyder A, McKinstry R, Raichle M, Conturo T, Anatomic localization and quantitative analysis of gradient refocused echo-planar fMRI susceptibility artifacts, NeuroImage 6 (1997) 156–167. [PubMed: 9344820]

[27]. Uğurbil K, Xu J, Auerbach EJ, Moeller S, Vu A, Duarte-Carvajalino J, Lenglet C, Wu X, Schmitter S, Van de Moortele PF, Strupp J, Sapiro G, De Martino F, Wang D, Harel N, Garwood M, Chen Feinberg L, Smith SM, Miller KL, Sotiropoulos S, Jbabdi S, Andersson JL, Behrens T, Glasser M, Van Essen D, Yacoub E, Pushing spatial and temporal resolution for functional and diffusion MRI in the Human Connectome Project, NeuroImage 80 (2013)80–104. [PubMed: 23702417]

[28]. Glasser M, Sotiropoulos S, Wilson J, Coalson T, Fischl B, Andersson J, Xu J, Jbabdi S, Webster M, Polimeni J, Van Essen D, Jenkinson M, for the WUMinn HCP Consortium, The minimal preprocessing pipelines for the Human Connectome Project, NeuroImage 80 (2013) 105–124. [PubMed: 23668970]

[29]. Van Dijk K, Hedden T, Venkataraman A, Evans K, Lazar S, Buckner R, Intrinsic functional connectivity as a tool for human connectomics: theory, properties, and optimization, J. Neurophysiol 103 (1) (2010) 297–321. [PubMed: 19889849]

[30]. Smith S, Beckmann C, Anderson J, Auerbach E, Bijsterbosch J, Douaud G, Duff E, Feinberg D, Griffanti L, Harms M, Kelly M, Laumann T, Miller K, Moeller S, Petersen S, Power J, Salimi-Khorshidi G, Snyder AZ, Vu AT, Woolrich MW, Xu J, Yacoub E, Uğurbil K, Van Essen D, Glasser M, for the WUMinn HCP Consortium, Resting-state fMRI in the Human Connectome Project, NeuroImage 80 (2013) 144–168. [PubMed: 23702415]

[31]. Fox M, Zhang D, Snyder A, Raichle M, The global signal and observed anticorrelated resting state brain networks, J. Neurophysiol 101 (2009) 3270?3283. [PubMed: 19339462]

[32]. He H, Liu T, A geometric view of global signal confounds in resting-state functional MRI, NeuroImage 59 (2012) 2339?2348. [PubMed: 21982929]

[33]. Fischl B, Freesurfer, NeuroImage 62 (2) (2012) 774–781. [PubMed: 22248573]

[34]. Parkes L, Schwarzbach J, Bouts A, Pullens P, Kerskens C, Norris D, Quantifying the spatial resolution of the gradient echo and spin echo BOLD response at 3 Tesla, Magnetic Resonance in Medicine 54 (6) (2005)1465–1472. [PubMed: 16276507]

[35]. Thielscher A, Kammer T, Electric field properties of two commercial figure-8 coils in tms: calculation of focality and efficiency, Clinical neurophysiology 115 (2004) 1697–1708. [PubMed: 15203072]

[36]. Welvaert M, Rosseel Y, On the definition of signal-to-noise ratio and contrast-to-noise ratio for fmri data, PLOS ONE 8 (11) (2013) e77089. [PubMed: 24223118]

[37]. Anderson J, Ferguson M, Lopez-Larson M, Yurgelun-Todd D, Reproducibility of single-subject functional connectivity measurements, American Journal of Neuroradiology 32 (3) (2011) 548–555. [PubMed: 21273356]

[38]. Choe AS, Jones CK, Joel SE, Muschelli J, Belegu V, Caffo BS, Lindquist MA, van Zijl PCM, Pekar JJ, Reproducibility and temporal structure in weekly resting-state fmri over a period of 3.5 years, PLOS ONE 10 (2015) 1–29.

[39]. Poldrack RA, Laumann TO, Koyejo O, Gregory B, Hover A, Chen M-Y, Gorgolewski KJ, Luci J, Joo SJ, Boyd RL, Hunicke-Smith S, Simpson ZB, Caven T, Sochat V, Shine JM, Gordon E,

Snyder AZ, Adeyemo B, Petersen SE, Glahn DC, Reese Mckay D, Curran JE, Göring HHH, Carless MA, Blangero J, Dougherty R, Leemans A, Handwerker DA, Frick L, Marcotte EM, Mumford JA, Long-term neural and physiological phenotyping of a single human, Nature Communications 6.

[40]. Shine JM, Koyejo O, Poldrack RA, Temporal metastates are associated with differential patterns of time-resolved connectivity, network topology, and attention, Proceedings of the National Academy of Sciences 113 (35) (2016) 9888–9891.

[41]. Wang J, Han J, Nguyen VT, Guo L, Guo CC, Improving the test- retest reliability of resting state fmri by removing the impact of sleep, Frontiers in Neuroscience 11 (2017) 249. [PubMed: 28533739]

[42]. Haber S, Knutson B, The reward circuit: linking primate anatomy and human imaging, Neuropsychopharmacology 35 (1) (2010) 4–26. [PubMed: 19812543]

[43]. Treadway M, Zald D, Reconsidering anhedonia in depression: lessons from translational neuroscience, Neuroscience and Biobehavioral Reviews 35 (3) (2011) 537–555. [PubMed: 20603146]

[44]. Der-Avakia A, Markou A, The neurobiology of anhedonia and other reward-related deficits, Trends in Neurosciences 35 (1) (2012) 68–77. [PubMed: 22177980]

[45]. Thomsen K, Whybrow P, Kringelbach M, Reconceptualizing anhedonia: novel perspectives on balancing the pleasure networks in the human brain, Frontiers in Behavioral Neuroscience 9 (2015) 49. [PubMed: 25814941]

[46]. Thielscher A, Opitz A, Windhoff M, Impact of the gyral geometry on the electric field induced by transcranial magnetic stimulation, NeuroImage 54 (1) (2011) 234–243. [PubMed: 20682353]

[47]. Brasil-Neto J, Cohen L, Panizza M, Nilsson J, Roth B, Hallett M, Optimal focal transcranial magnetic activation of the human motor cortex: effects of coil orientation, shape of the induced current pulse, and stimulus intensity, Journal of clinical neurophysiology 9 (1) (1992) 132–136. [PubMed: 1552001]

[48]. Thielscher A, Kammer T, Linking physics with physiology in TMS: a sphere field model to determine the cortical stimulation site in TMS, NeuroImage 17 (3) (2002) 1117–1130. [PubMed: 12414254]

[49]. Lee E, Duffy W, Hadimani R, Waris M, Siddiqui W, Islam F, Rajamani M, Nathan R, Jiles D, Investigational effect of brain-scalp distance on the efficacy of transcranial magnetic stimulation treatment in depression, IEEE Transactions on Magnetics 52 (2016) 7.

Highlights:

- The reproducibility of fcMRI-guided brain target in TMS is examined using HCP data.
- The inter-scan distance reduces from 37 mm in 15-min data to 25 mm in30-min data.
- A smoothing kernel with 12-mm FWHM is suggested to reduce inter-scan variabilities.

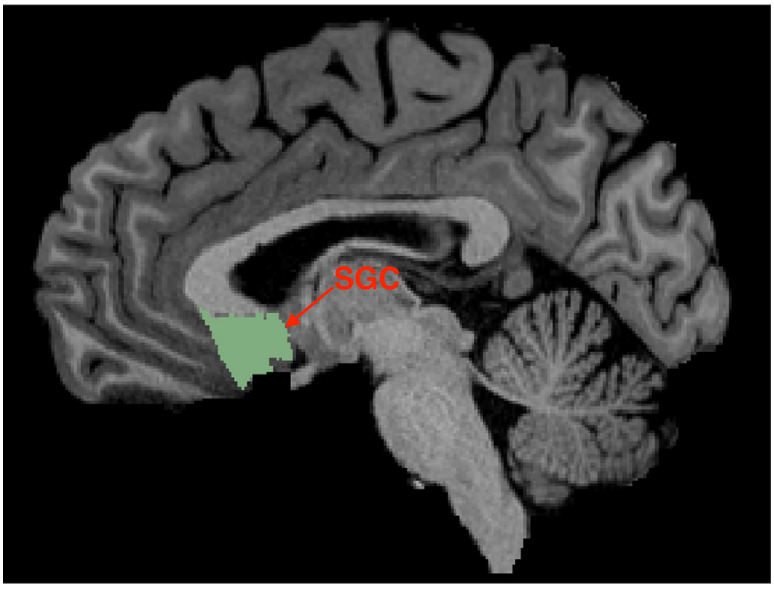

Figure 1:
An illustration of the selected SGC ROI of an HCP subject.

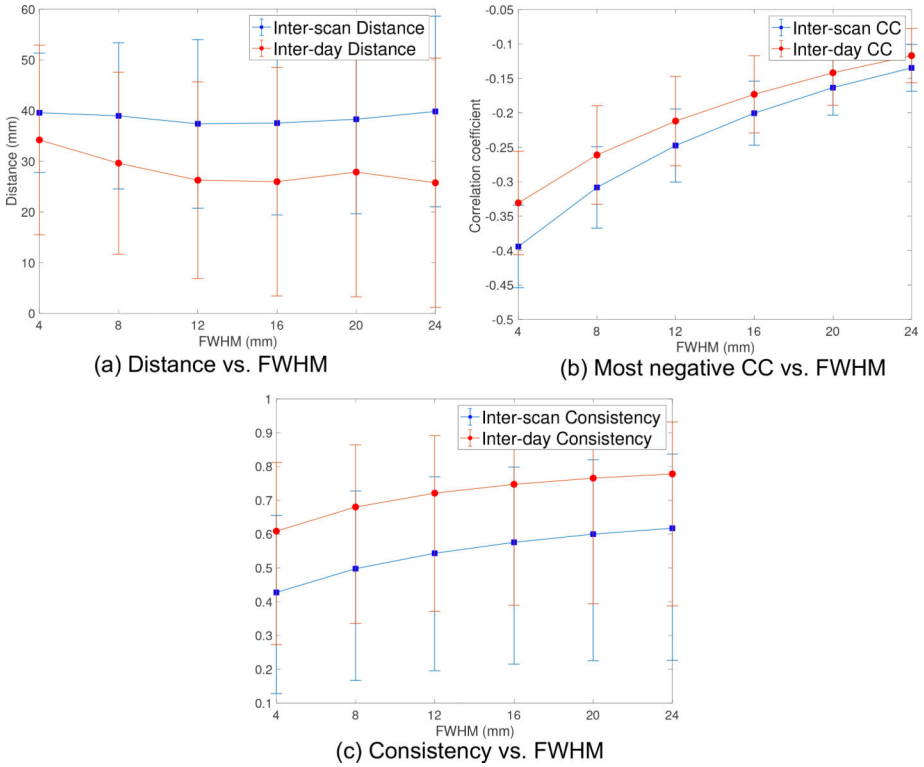

Figure 2:

(a) The inter-scan (15-min) and inter-day (30-min) distance measure between the most negative peaks of the SGC-DLPFC FC maps from the volume rsfMRI data of 100 HCP subjects, where the dashed lines are the corresponding ± standard deviation plots. (b) The corresponding correlation coefficient variability with FWHM smoothing kernel. (c) The consistency measure, which reflects the variability of SGC-DLPFC FC maps in the entire DLPFC region.

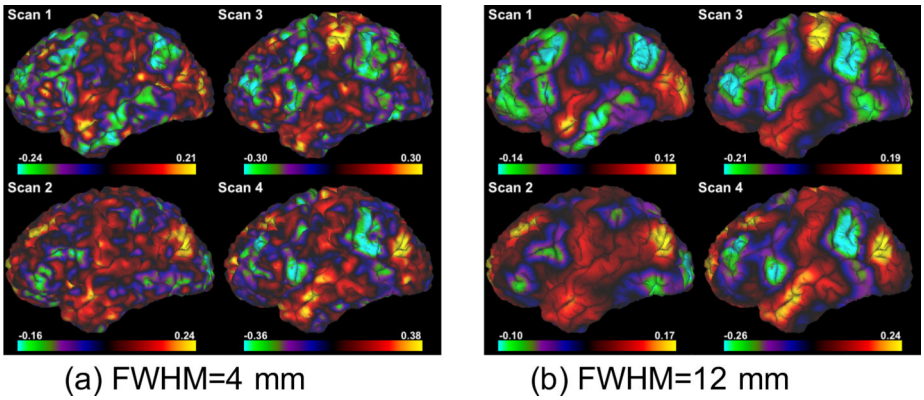

Figure 3:

Functional connectivity map of the left hemisphere with seed in the subgenual cingulate cortex (SGC) from 4 scans of the same subject smoothed by Gaussian kernels with different FWHM. Note that the location of the most negatively correlated region (green) is highly variable between the scans.

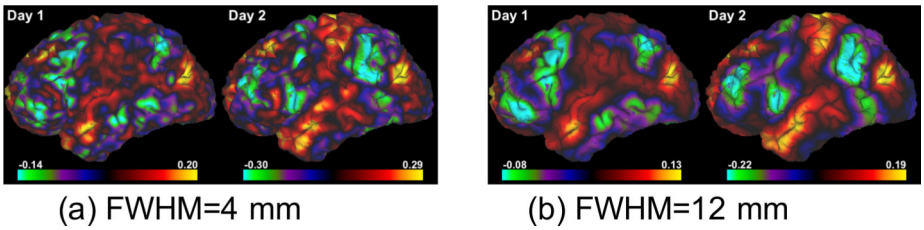

(a) FWHM=4 mm (b) FWHM=12 mm

Figure 4:

Functional connectivity map of the left hemisphere with seed in the subgenual cingulate cortex (SGC) from 2 different days of the same subject smoothed by Gaussian kernels with different FWHM.

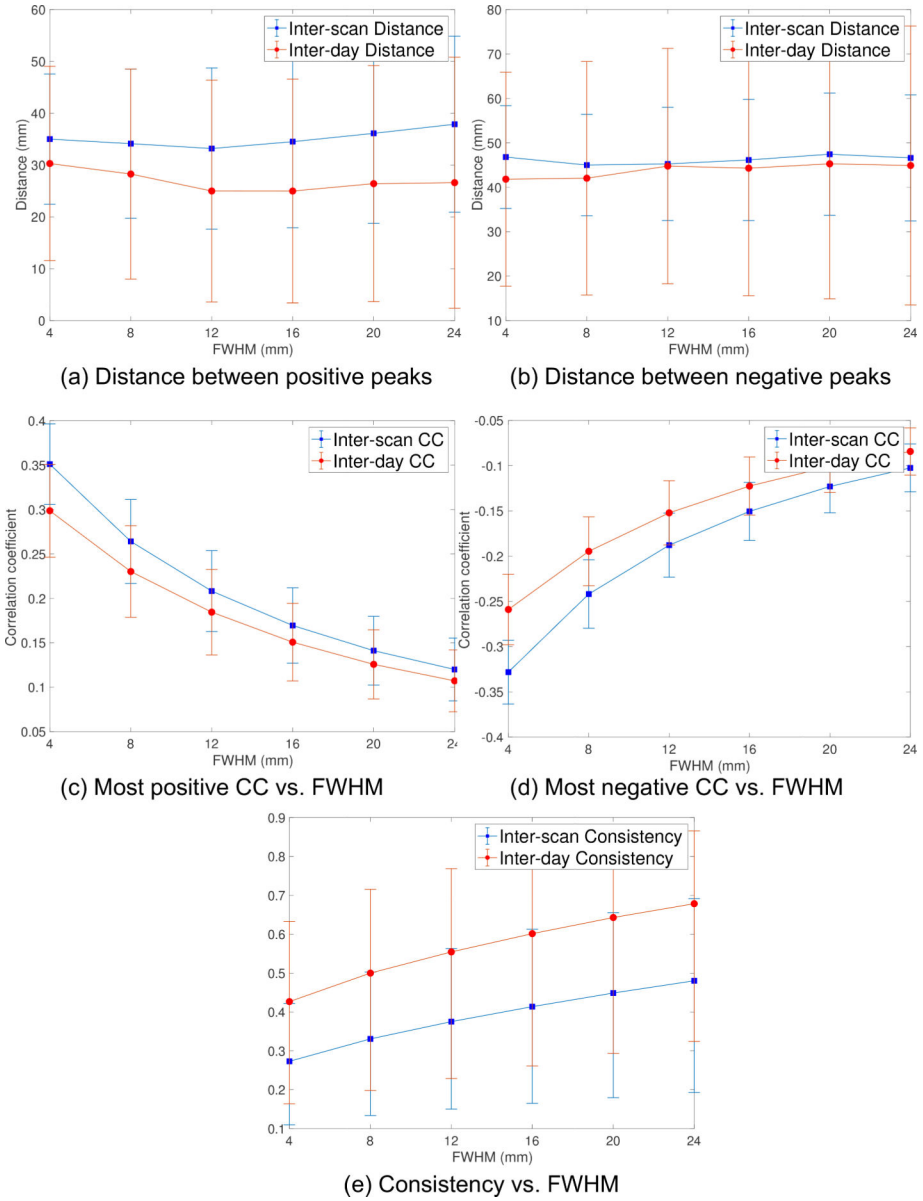

Figure 5:

(a) and (b) show the inter-scan (15-min) and inter-day (30-min) distance between the most positive and negative peaks of the NAc-DLPFC FC maps from the volume rsfMRI data, respectively. (c) and (d) illustrate the values of the most positive and negative CC, respectively. (e) shows the consistency measure, which reflects the variability of NAc-DLPFC FC maps in the entire DLPFC region.

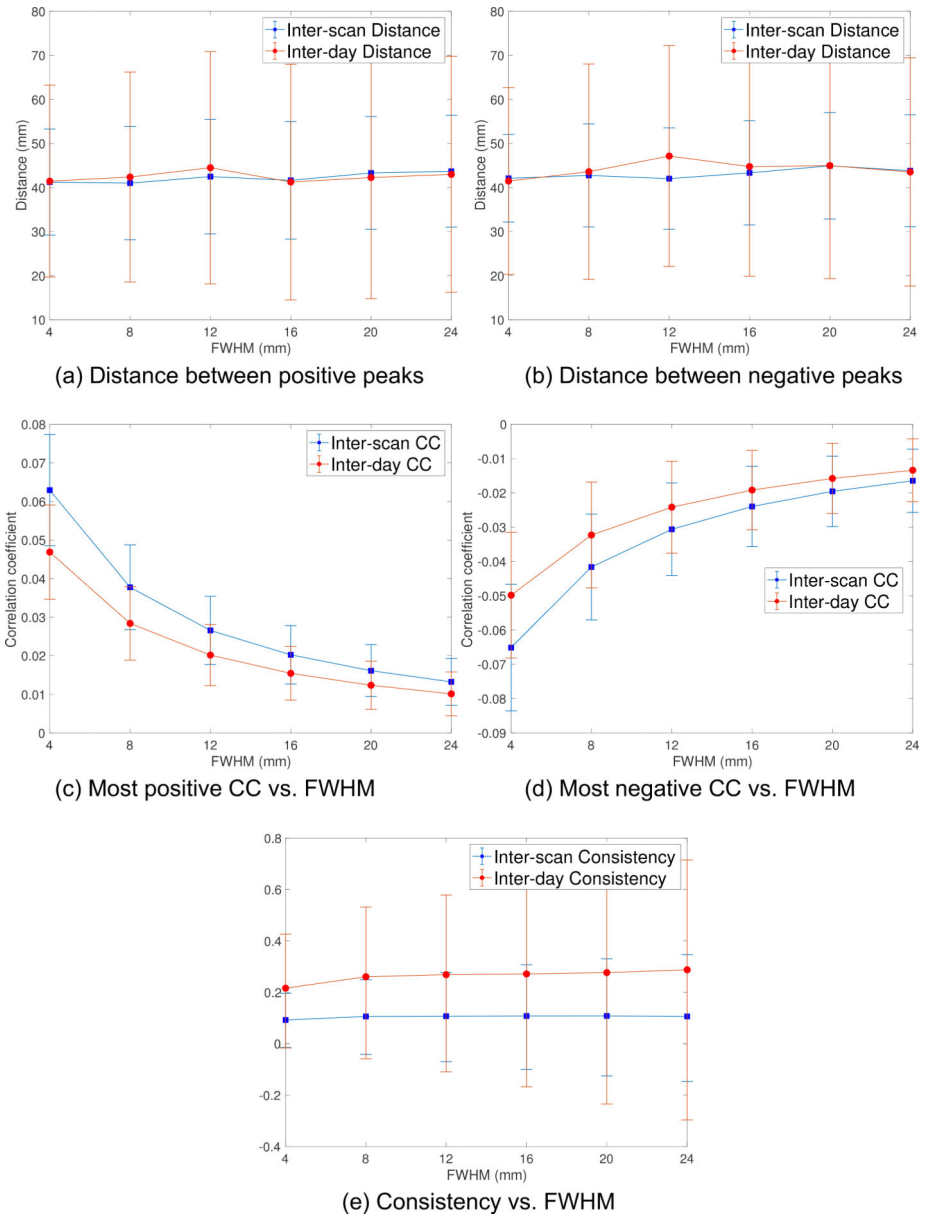

Figure 6:

(a) and (b) show the inter-scan (15-min) and inter-day (30-min) distance between the most positive and negative peaks of the NAc-DLPFC FC maps from the surface rsfMRI data, respectively. (c) and (d) illustrate the values of the most positive and negative CC, respectively. (e) shows the consistency measure, which reflects the variability of NAc-DLPFC FC maps in the entire DLPFC region.

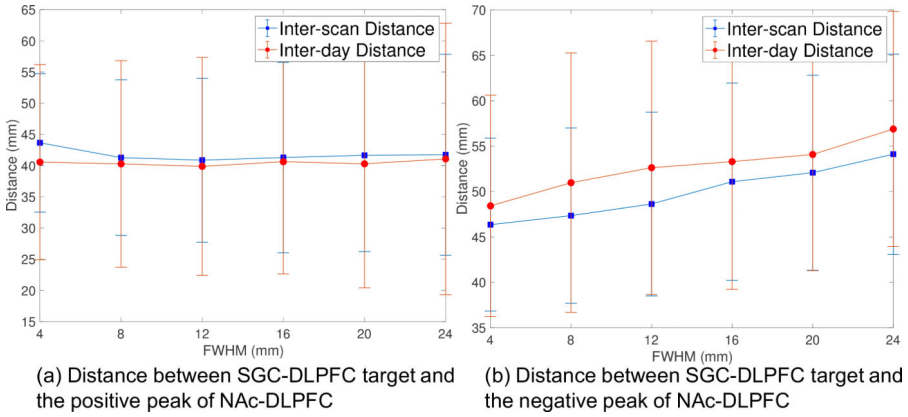

(a) Distance between SGC-DLPFC target and the positive peak of NAc-DLPFC

(b) Distance between SGC-DLPFC target and the negative peak of NAc-DLPFC

Figure 7:

(a) Distance between negative peaks of SGC-DLPFC FC maps and positive peaks of NAc-DLPFC FC maps. (b) Distance between negative peaks of SGC-DLPFC FC maps and positive peaks of NAc-DLPFC FC maps.